Interactions of Metal Ions with Phosphatidylserine Bilayer Membranes: Effect of Hydrocarbon Chain Unsaturation†

Jairajh Mattai,‡ Helmut Hauser,§ Rudy A. Demel,∥ and G. Graham Shipley*,‡

Laboratorium für Biochemie, Eidgenössische Technische Hochschule Zürich, CH-8092 Zürich, Switzerland, Laboratory of Biochemistry, State University of Utrecht, Utrecht, The Netherlands, and Biophysics Institute, Departments of Medicine and Biochemistry, Boston University School of Medicine, Housman Medical Research Center, Boston, Massachusetts 02118

Received August 30, 1988; Revised Manuscript Received November 2, 1988

ABSTRACT: A combination of surface monolayer, scanning calorimetry, ^{31}P NMR, and spin-label ESR techniques has been used to monitor the interactions of monovalent (NH_4^+, Na^+, and Li^+) and divalent (Ca^{2+}) cations with phosphatidylserines (PS) differing in their levels of chain unsaturation. Comparisons are made between the disaturated dimyristoyl-, dipalmitoyl-, and dihexadecyl-PS (DMPS, DPPS, and DHPS), saturated cis-monounsaturated palmitoyloleoyl-PS (POPS) (and bovine brain PS), di-trans-monounsaturated dielaidoyl-PS (DEPS), and di-cis-monounsaturated dioleoyl-PS (DOPS). Na^+ and NH_4^+ cations interact weakly with all PS monolayers and bilayers without significant changes in molecular conformation, chain packing, or headgroup dynamics and without dependence on chain composition. In contrast, considering these structural and dynamic parameters, Li^+ shows a gradation in its interaction with PS (DMPS > POPS $\sim$ bovine brain PS > DOPS), suggesting that Li^+–PS interactions depend on the interfacial properties of the PS molecules (e.g., surface area). Finally, Ca^{2+} interacts strongly with all PS monolayers and bilayers, without obvious chain selectivity. Thus, ion binding to PS depends not only on the properties of the cation (Na^+ vs Li^+ vs Ca^{2+}) but also on the molecular details of the PS membrane surface.

Phosphatidylserine (PS)[1] is the major anionic phospholipid in many mammalian cell membranes. Due to its net negative charge at physiological pH, the interactions of PS with monovalent and divalent cations may be involved in membrane-associated processes such as lipid phase modulation or phase separation, fusion events, blood clotting factor binding, enzyme regulation, etc. Thus, a number of studies of cation binding to model membranes of PS (usually isolated from bovine brain) have been performed (Abramson et al., 1964; Papahadjopoulos & Miller, 1967; Hauser & Phillips, 1973; Atkinson et al., 1974; Jacobson & Papahadjopoulos, 1975; Puskin, 1977; Hauser et al., 1977; Papahadjopoulos et al., 1977, 1978; Newton et al., 1978; Eisenberg et al., 1979; Ohki & Kurland, 1981; McLaughlin et al., 1981; McLaughlin, 1982; Ohki et al., 1982; Loosley-Millman et al., 1982; Feigenson, 1986). More recently, the availability of synthetic PS with controlled fatty acyl chain composition has resulted in an improved understanding of the structure and properties of PS bilayers and their interactions with cations (MacDonald et al., 1976; Luna & McConnell, 1977; van Dijck et al., 1978; Browning & Seelig, 1980; Cevc et al., 1981; Hauser et al., 1982a; Hauser & Shipley, 1981, 1983, 1984, 1985; Feigenson, 1986). The careful study of Feigenson (1986) is particularly valuable in defining the stoichiometry of the complex formed by Ca^{2+} with different PS. For POPS, DOPS, and bovine brain PS, the stoichiometry found is always $Ca(PS)_2$.

Our own studies have focused on the structure and thermotropic properties of a homologous series of saturated-chain PS in the absence and presence of monovalent and divalent cations. Using primarily differential scanning calorimetry (DSC) and X-ray diffraction, we have shown that saturated-chain PS form continuously swelling, hydrated bilayers exhibiting chain length dependent gel → liquid-crystal transitions (Hauser et al., 1982a). Monovalent cations such as Na^+ and K^+ produce only minor changes in PS bilayer structure, stability, and chain packing (Hauser & Shipley, 1981, 1983) but, as a consequence of ion-induced shielding of the negatively charged bilayer surface, reduce the interlayer separation of bilayers with a dependence on ionic strength. In contrast, the monovalent cation Li^+ and the divalent cations Mg^{2+} and Ca^{2+}, all with relatively small ionic radii, form dehydrated, high-melting metal ion–PS complexes and produce bilayer hydrocarbon chain crystallization (Hauser & Shipley, 1981, 1983, 1984, 1985).

Since PS with saturated chains at both the *sn*-1 and *sn*-2 positions do not occur in natural membranes, we have been interested in exploring the effect of chain unsaturation on PS interactions with metal ions. In particular, since chain unsaturation can be expected to increase the surface area occupied at the lipid–water interface and thus the intermolecular separation at the interface of the charged molecular groups (PO_4^-, $-CO_2^-$, and $-NH_3^+$) presumably involved in ion binding, physical studies of unsaturated-chain PS have been initiated. In this study, we compare the properties of PS with one or two unsaturated chains and their interactions with Li^+, Na^+, and Ca^{2+} with the previously studied saturated-chain PS. The methods used include surface monolayers, DSC, ^{31}P NMR, and spin-label ESR.

† This research was supported by Research Grant HL-26335 and Training Grant HL-07291 from the National Institutes of Health and by a grant from the Swiss National Science Foundation (3.579-0.84). In addition, this research was greatly facilitated by a grant from the National Science Foundation (INT-84-05038).

‡ Boston University School of Medicine.
§ Eidgenossiche Technische Hochschule Zürich.
∥ State University of Utrecht.

[1] Abbreviations: PC, phosphatidylcholine; PS, phosphatidylserine; DLPS, dilauroylphosphatidylserine; DMPS, dimyristoylphosphatidylserine; DPPS, dipalmitoylphosphatidylserine; DHPS, dihexadecylphosphatidylserine; DSPS, distearoylphosphatidylserine; POPS, 1-palmitoyl-2-oleoylphosphatidylserine; DOPS, dioleoylphosphatidylserine; DEPS, dielaidoylphosphatidylserine; DSC, differential scanning calorimetry; TLC, thin-layer chromatography; EDTA, ethylenediaminetetraacetic acid; Tris, tris(hydroxymethyl)aminomethane.

0006-2960/89/0428-2322$01.50/0

Materials and Methods

Materials

DMPS, DPPS, DSPS, POPS, and DOPS were synthesized as described previously (Hermetter et al., 1982). DEPS was synthesized according to Comfurius and Zwaal (1977). The ether-linked DHPS was synthesized by R. Berchtold (Biochemische Lab., Berne, Switzerland). Bovine brain PS was purchased from Lipid Products (Surrey, U.K.) and used without further purification. Spin-labeled phosphatidylcholine, 1-palmitoyl-2-(8-doxylpalmitoyl)-3-*sn*-phosphatidylcholine (8-doxyl-PC), was prepared from 1,2-dipalmitoyl-3-*sn*-phosphatidylcholine as described by Hauser et al. (1982b). The stearic acid spin-label with the 4,4-dimethyl-3-oxazolidinyl-1-oxy group (doxyl group) attached to C-5 (5-doxylstearic acid) and its methyl ester were purchased from Syva (Palo Alto, CA). NH_4Cl, alkali metal chlorides, and $CaCl_2$ (Puriss grade) were obtained from Merck (Rahway, NJ). All other chemicals used were analytical grade. The lipids used were shown to be pure by TLC methods using several solvent systems (Hauser et al., 1982a), and by chemical microanalysis. The acid form of PS was converted into the monoammonium salt as described previously (Hauser et al., 1982a). Alternatively, the conversion of the acid form into different salt forms and vice versa was carried out according to the method of Bligh and Dyer (1959).

Methods

Surface Monolayers. Surface pressure–area isotherms were measured at the air–water interface at 22 °C using a Teflon trough (32.2 cm × 17.2 cm) which was placed within a thermostated box; 50 nmol of lipid dissolved in $CHCl_3$/CH_3OH (4:1 v/v) was carefully spread at the air–water interface from an Agla microsyringe. The surface tension was determined with a recording Beckman LM 500 electrobalance, and pressure–area curves were recorded at a compression rate of 0.258 $nm^2\ mol^{-1}\ min^{-1}$. The reproducibility was better than 1 $Å^2$/molecule. The following buffers were used: 0.066 M phosphate buffer (Na_2HPO_4, KH_2PO_4), pH 7.4; 5 mM Tris buffer, pH 7.4; and 0.2 M borate buffer (H_3BO_3, $Na_2B_4O_7$), pH 7.4.

Scanning Calorimetry. Hydrated samples for differential scanning calorimetry (DSC) were prepared by weighing the solid PS (3–5 mg) into the DSC pan and adding the appropriate amount of aqueous buffer, usually 50 μL, with a Hamilton syringe or gravimetrically. The pan was immediately sealed and transferred to the calorimeter. For bovine brain PS, a $CHCl_3$/CH_3OH (2:1 v/v) solution was injected into the DSC pan, and after evaporation of the organic solvent, the lipid was dried to constant weight. Unless otherwise stated, the PS was dispersed in 5 mM phosphate buffer, pH 7.0, containing 5 mM EDTA. For studying the effect of salt on the DSC behavior of PS, the appropriate amount of salt was added to the buffer used to disperse the dry PS.

Calorimetric measurements were carried out with a Perkin-Elmer (Norwalk, CT) DSC-2 differential scanning calorimeter. Each sample was heated and cooled repeatedly, usually at a rate of 5 °C/min. The peak in the excess apparent heat capacity vs temperature plot was taken as the transition temperature, T_c. Transition temperatures and enthalpies were determined by using a Perkin-Elmer Model 3600 data station.

^{31}P NMR Measurements. Unless otherwise stated, samples for ^{31}P NMR measurements were prepared by evaporating the PS solution in $CHCl_3$/CH_3OH (2:1 v/v) in a round-bottom flask and drying the lipid film in a vacuum. The PS was dispersed in 5 mM Tris buffer, pH 7.0, which, if required, contained the appropriate amount of salt, to give usually a 0.12–0.15 M PS dispersion. Dispersions of POPS were 0.04–0.12 M because less of this PS was available. The salt concentrations used were high (usually >0.5 M) in order to shift the equilibrium to favor formation of the metal ion–PS complex. The PS–metal ion precipitate formed under these conditions was spun down at 4000 rpm for 20 min and transferred into the NMR tube (5-mm diameter, ~2.5 cm long). The PS–metal ion precipitates thus formed are referred to as "aqueous" precipitates; these are contrasted with "anhydrous" PS–metal ion complexes obtained by vacuum drying the "aqueous" precipitates.

Proton-decoupled ^{31}P NMR powder spectra of PS–metal ion complexes were recorded on a Bruker CXP-300 Fourier-transform spectrometer operating at 121.46 MHz. Axially symmetric ^{31}P powder spectra of liquid-crystalline phospholipid dispersions were recorded by using the simple 90° pulse, double-resonance method. Crystalline samples giving rise to axially asymmetric powder spectra were recorded by using the cross-polarization, double-resonance technique (Pines et al., 1973). Liquid-crystalline bilayer samples required 500–1000 free induction decays and crystalline bilayer samples 2000–5000. All measurements were carried out at room temperature. Chemical shielding data were referenced to external 85% orthophosphoric acid. The error in determining the width of the powder spectra is 3–5 ppm, larger errors being due to ^{31}P powder spectra with less well-defined edges.

ESR Measurements. Spin-labeled dispersions for ESR measurements were prepared by mixing the PS and the spin-label in $CHCl_3$/CH_3OH (2:1 v/v) followed by solvent removal under vacuum. The PS concentrations used varied between 0.014 and 0.05 M; the PS:spin-label molar ratio was usually 100:1. The dry PS/spin-label film was dispersed in 5 mM Tris buffer, pH 7.0; 50 μL of the PS dispersion was injected into a 1-mm glass capillary used for the ESR measurements. If required, 16 μL of a concentrated salt solution (NaCl, LiCl, or $CaCl_2$) in the same buffer was added, the capillary was sealed, and its contents were thoroughly mixed. The PS precipitate formed upon the addition of salt was spun down in the capillary at 4000 rpm for ~20 min. An excess of salt was used in these experiments in order to shift the equilibrium toward the PS–metal ion complex. In this way, ESR spectra characteristic of the metal ion–PS complexes were obtained rather than mixed spectra from free and complexed PS.

ESR spectra were recorded at 9.2 GHz with a Varian X-band spectrometer (Model E-104A) equipped with a variable-temperature control. The temperature was monitored with a thermocouple and was accurate to ±1 °C. ESR spectra were recorded with a microwave power of about 10 mW; the amplitude of the 100-kHz field modulation was 1 G; the magnetic field sweep was 100–200 G.

Results

Surface Monolayers. At room temperature, DPPS spread on 0.066 M phosphate buffer, pH 7.4, gives a condensed monolayer with a limiting area of 40.5 $Å^2$/molecule (Figure 1A, curve 2). The pressure–area curve of the ether-linked DHPS (Figure 1A, curve 1) is similar to that of DPPS (below 30 mN/m, DHPS is even more condensed) and has an identical limiting area (40.5 $Å^2$). Good agreement in the surface behavior of ester- and ether-linked phosphatidylcholines has also been reported (Paltauf et al., 1971). At room temperature, the shorter chain DMPS undergoes a two-dimensional phase transition from the liquid-expanded to the liquid-condensed state at 21.6 mN/m and a molecular area of 59

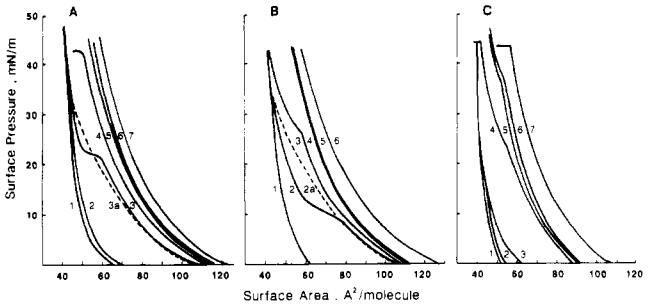

FIGURE 1: Surface pressure–molecular area curves for PS differing in degree and type of chain unsaturation. (A) Monolayers were spread on 0.066 M phosphate buffer, pH. 7.4. PS were spread as the monosodium salts unless otherwise stated. (1) DHPS; (2) DPPS; (3) DMPS; (3a) for comparison, DMPS spread on 5 mM Tris-HCl, pH 7.4; (4) DEPS; (5) bovine brain PS; (6) POPS (as the NH_4^+ salt); (7) DOPS. (B) Monolayers were spread on 5 mM Tris-HCl, pH 7.4, containing 100 mM LiCl. (1) DPPS; (2) DMPS; (2a) for comparison, DMPS spread on 5 mM Tris-HCl, pH 7.4; (3) DEPS; (4) bovine brain PS; (5) POPS; (6) DOPS. (C) Monolayers were spread on 5 mM Tris-HCl, pH 7.4, containing 10 mM $CaCl_2$. (1) DHPS; (2) DPPS; (3) DMPS; (4) DEPS; (5) bovine brain PS; (6) POPS; (7) DOPS.

Table I: Molecular Areas (Å²/Molecule) of Different Phosphatidylserines[a]

phosphatidyl-serine	molecular area (Å²/molecule) phosphate buffer	Tris-HCl buffer	Tris-HCl buffer + 100 mM LiCl	Tris-HCl buffer + 10 mM $CaCl_2$
DMPS	45.5	46.5	45.5	40.2
DPPS	44.2	44.4	43.2	40.2
DHPS	43.5	nd[b]	43.0	40.2
POPS	63.7	63.7	62.1	56.6
bovine brain PS	62.0	62.4	61.5	54.7
DEPS	57.2	57.3	52.0	48.0
DOPS	67.5	67.5	67.2	62.5

[a] Phosphatidylserine monolayers were spread on (1) 0.066 M phosphate buffer, pH 7.4, on (2) 5 mM Tris-HCl, pH 7.4, and (3) on Tris-HCl, pH 7.4, containing either 100 mM LiCl or 10 mM $CaCl_2$. The molecular areas were derived from the surface pressure–area curves at 30 mN/m. [b] nd, not determined.

Å²/molecule (Figure 1A, curve 3). However, the limiting area of DMPS (40.5 Å²) is identical with that of DPPS and DHPS. Introduction of the cis-monounsaturated oleoyl chain at the *sn*-2 position (POPS) results in a liquid-expanded monolayer over the whole pressure range (Figure 1A, curve 6). At 30 mN/m (see Table I), the molecular area of POPS (64 Å²) is increased by 20 Å²/molecule compared to DPPS (44 Å²). Note, however, that the area of a condensed monolayer (DPPS) is being compared with that of an expanded monolayer (POPS). PS with a cis-monounsaturated chain at both the *sn*-1 and *sn*-2 positions (DOPS) results in a further, albeit smaller, increase in molecular area to 67.5 Å² (ΔA = 3.8 Å²/molecule) at 30 mN/m (Figure 1A, curve 7). The interfacial properties of bovine brain PS are similar to those of POPS (cf. Figure 1A, curves 5 and 6). DEPS with trans-monounsaturated chains at both *sn*-1 and *sn*-2 positions also exhibits a liquid-expanded monolayer but with a smaller area per molecule than both DOPS and POPS at the same pressure (Figure 1A, curve 4). The smaller limiting molecular area observed with the trans-unsaturated DEPS indicates increased packing order compared to the corresponding cis-unsaturated DOPS. The pressure–area curve of DEPS exhibits a sharp collapse at 43 mN/m. Its limiting molecular area of 50.7 Å²/molecule is intermediate between those of DPPS and DOPS (see Figure 1).

Essentially identical pressure–area curves to those shown in Figure 1 are obtained for the different PS spread on 5 mM Tris buffer, pH 7.4 (data not shown, but see comparison of molecular areas at 30 mN/m in Table I), the only exception being DMPS (see Figure 1A, curve 3a). For DMPS, the two-dimensional phase transition appears to be much broader and less defined in the presence of Tris buffer, although other features like the initial (liftoff) area of 105 Å²/molecule and the limiting area of 41 Å²/molecule agree well with those of DMPS monolayers spread on phosphate buffer (cf. Figure 1A, curves 3 and 3a).

With the exception of DMPS and DEPS, the presence of 0.1 M LiCl in the subphase has little effect on the pressure–area curves of the different PS spread on Tris buffer (see Figure 1B and Table I). Both liquid-condensed (DPPS; see Figure 1B, curve 1) and liquid-expanded (bovine brain PS, POPS, and DOPS; see Figure 1B, curves 4–6) monolayers show a small reduction (~1 Å²) in area for molecule in the presence of Li^+ (cf. molecular areas at 30 mN/m in Table I). DMPS shows a very broad two-dimensional liquid-expanded ↔ liquid-condensed phase transition in the absence of LiCl (Figure 1B, curve 2a); in the presence of 0.1 M LiCl, a liquid-expanded ↔ liquid-condensed phase transition is clearly observed at 8.8 mN/m (Figure 1B, curve 2). For DEPS, a significant condensation is observed in the presence of Li^+ (Figure 1B, curve 3), and a two-dimensional transition is observed at 26 mN/m; thus, at 30 mN/m, the area is reduced by 5.3 Å² (Table I).

The effect of 10 mM $CaCl_2$ upon monolayers of PS differing in the degree and type of chain unsaturation is depicted in Figure 1C. $CaCl_2$ concentrations in excess of 5 mM have a marked effect on the molecular packing of all PS monolayers spread on Tris buffer. DHPS, DPPS, and DMPS (Figure 1C, curves 1, 2, and 3, respectively) all give condensed monolayers with a limiting area of 40 Å²/molecule, but with reduced areas compared to those observed in the absence of Ca^{2+} (cf. Figure 1A,C and see Table I) at identical pressures. Most interesting is the complete elimination of the two-dimensional phase transition of DMPS in the presence of $CaCl_2$ (Figure 1C, curve 3). Identical pressure–area curves are obtained when DMPS is spread on 5 mM Tris or 5 mM borate buffer, both at pH 7.4, and containing 10 mM $CaCl_2$. The liquid-expanded monolayers of bovine brain PS and POPS show specific condensation (by 7–8 Å²/molecule at 30 mN/m, see Table I) in the presence of 10 mM $CaCl_2$ (Figure 1C, curves 5 and 6). Furthermore, monolayers of both bovine brain PS and POPS exhibit a transition at ~36 mN/m in the presence of 10 mM $CaCl_2$, and the limiting area at 44 mN/m is 47.5 Å²/molecule (Figure 1C, curves 5 and 6). DEPS also shows area condensation and a transition at 26 mN/m with a limiting molecular area of 42 Å²/molecule at 44 mN/m (Figure 1C, curve 4). In this case, the limiting molecular area is quite close to that of the saturated PS, indicating that under these conditions the trans-unsaturated chains are in a nearly all-trans conformation. Although DOPS with the cis-monounsaturated chains forms liquid-expanded monolayers both in the absence and in the presence (Figure 1C, curve 7) of 10 mM $CaCl_2$, in the presence of Ca^{2+} the molecular area is significantly reduced, for example by 5 Å²/molecule at 30 mN/m (Table I). The pressure–area isotherm shows a sharp collapse at 43.6 mN/m at which point the limiting molecular area is 57 Å²/molecule. This is significantly higher than the limiting area of trans-monounsaturated DEPS, 44 Å²/molecule (cf. Figure 1C, curves 7 and 4).

Differential Scanning Calorimetry. The thermotropic behavior of PS with saturated fatty acyl chains and their com-

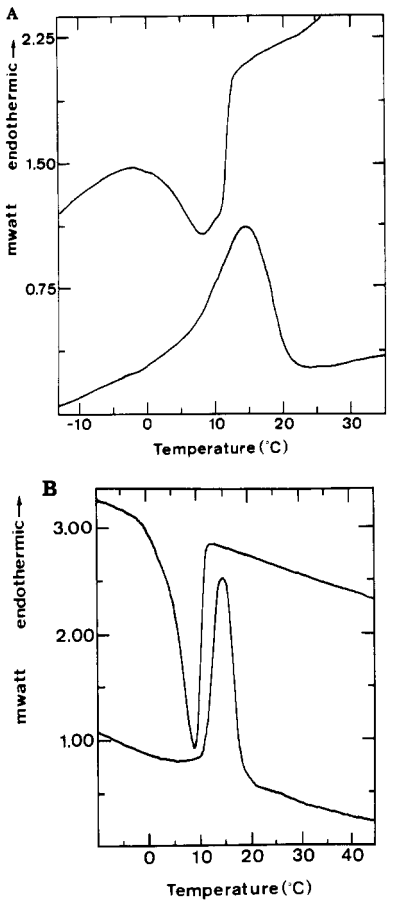

FIGURE 2: (A) DSC heating and cooling curves of bovine brain PS (Na^+ salt; 60 mg/mL = 0.072 M) dispersed in 5 mM sodium phosphate buffer (pH 7.0; 5 mM EDTA). Heating and cooling curves were recorded at 5 °C/min. (B) DSC heating curves of POPS (Na^+ salt; 80 mg/mL = 0.099 M) dispersed in 5 mM sodium phosphate buffer (pH 7.0; 5 mM EDTA). Heating and cooling curves were recorded at 5 °C/min.

plexes with Li^+ and Ca^{2+} was reported previously (Hauser et al., 1982a; Hauser & Shipley, 1981, 1983, 1984). All monovalent alkali metal ions except Li^+ have rather small effects on the gel to liquid-crystal transition temperature of saturated-chain PS. In contrast, excess Li^+ produces a dramatic increase in transition temperature and enthalpy of DLPS, DMPS, and DPPS (Hauser & Shipley, 1983). For example, in the presence of excess Li^+, the transition temperature of DMPS is increased by 50 °C, and the transition enthalpy ΔH is more than twice that observed in the presence of other monovalent cations, e.g., Na^+ or K^+. Excess Ca^{2+} also forms stable, high-melting complexes with DLPS, DMPS, DPPS, and DSPS which exhibit broad endothermic transitions at temperatures between 151 and 157 °C (Hauser & Shipley, 1984).

The monosodium salt of bovine brain PS in sodium phosphate buffer gives a broad, asymmetric gel to liquid-crystal transition (T_c) at 14 ± 1 °C, ΔH = 6.2 ± 0.7 kcal/mol) (Figure 2A). Upon cooling, a broad exotherm is observed with the peak maximum depressed by 5.6 °C compared to the transition temperature observed on heating. Both the endothermic and exothermic transitions are reproducible in successive heating and cooling cycles. The effect of Li^+ on bovine brain PS is shown in Figure 3A,B. With increasing Li^+ concentration, T_c increases progressively, and at $[Li^+] > 0.5$ M, a second transition appears at 52 °C. With increasing $[Li^+]$ up to 1 M, the temperature of both transitions increases (Figure 3A,B), and the enthalpy of the high-temperature

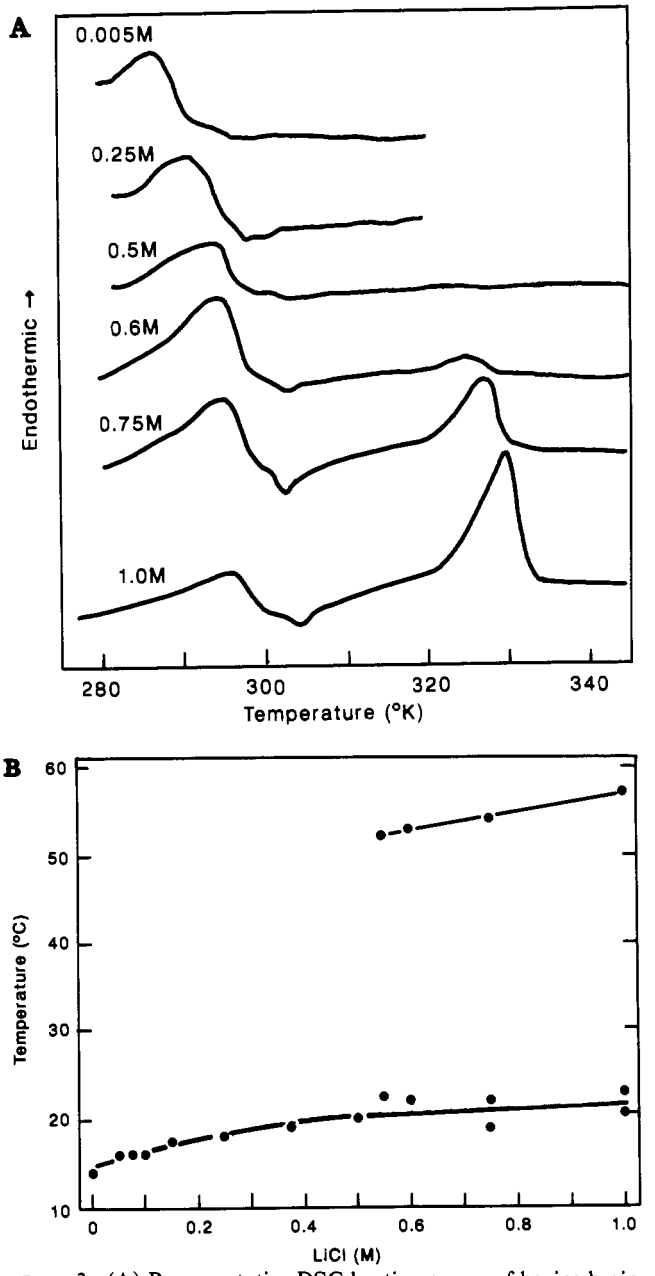

FIGURE 3: (A) Representative DSC heating curves of bovine brain PS (Na^+ salt; 60 mg/mL = 0.072 M) dispersed in 5 mM sodium phosphate buffer (pH 7.0; 5 mM EDTA) as a function of the LiCl concentration. Heating curves (5 °C/min) are shown for 5 mM Li^+, 0.25 M Li^+, 0.5 M Li^+, 0.6 M Li^+, 0.75 M Li^+, and 1 M Li^+ (top to bottom). (B) Transition temperatures of bovine brain PS (Na^+ salt) as a function of the LiCl concentration. Peak maxima derived from DSC heating curves as shown in (A) are plotted.

transition increases at the expense of the low-temperature transition. In addition, a small exotherm is observed at ~30 °C. Even at the highest $[Li^+]$, 1 M, the low-temperature transition is still present. This behavior differs somewhat from that of Li^+–DMPS, although both exhibit Li^+-induced high-melting transitions. At $[Li^+]$ = 0.5 M, the low-temperature transition of DMPS was barely detectable, and at concentrations in excess of 0.5 M, it had disappeared completely (Hauser & Shipley, 1981, 1983). In spite of repeated cycling through the chain-melting transition, in some cases access of Li^+ (and Ca^{2+}, see below) to all potential binding sites appears to be restricted. A partial explanation may be that the formation of stacked, "dehydrated" Li^+–PS (or Ca^{2+}–PS) multibilayers restricts access of cations to some polar group sites on PS.

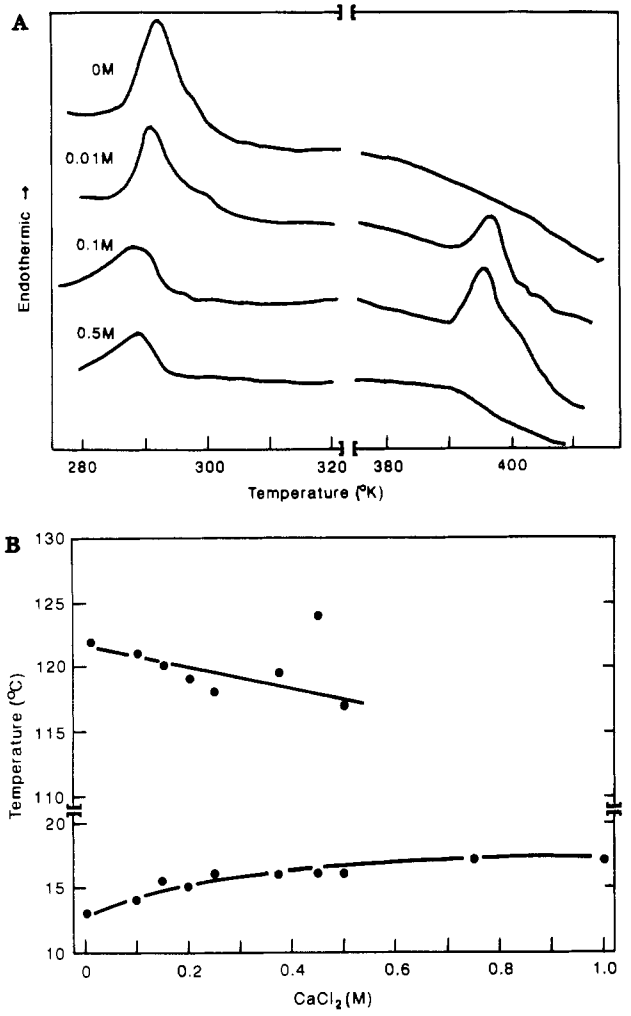

FIGURE 4: (A) Representative DSC heating curves of bovine brain PS (Na^+ salt; 60 mg/mL = 0.072 M) dispersed in 5 mM phosphate buffer (pH 7.0; 5 mM EDTA) as a function of $CaCl_2$ concentration. Heating curves (5 °C/min) are shown for bovine brain PS without Ca^{2+} and for 0.01 M Ca^{2+}, 0.1 M Ca^{2+}, and 0.5 M Ca^{2+} (top to bottom). (B) Transition temperatures of bovine brain PS (Na^+ salt) as a function of the $CaCl_2$ concentration. Peak maxima derived from the DSC heating curves as shown in (A) are plotted.

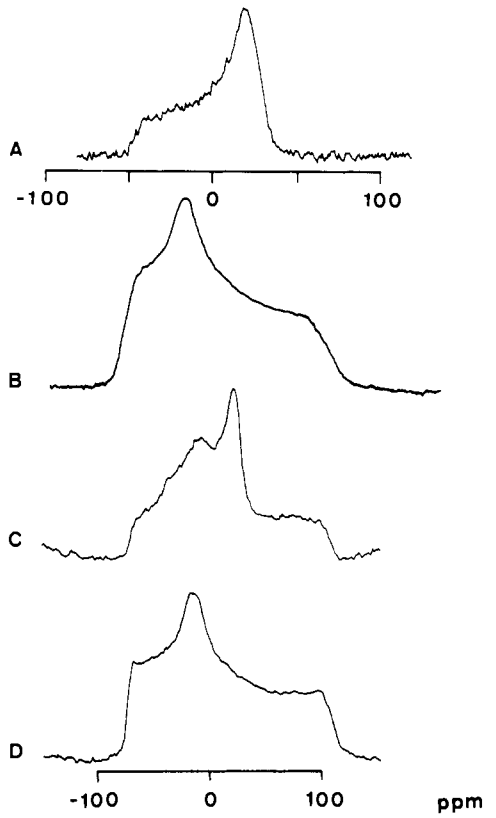

FIGURE 5: Proton-decoupled ^{31}P NMR powder spectra of DMPS–metal ion complexes recorded at 121.46 MHz at room temperature. Spectra were taken of aqueous precipitates of DMPS (0.13 M) formed in the presence of excess cations as described under Materials and Methods. (A) NaCl concentration = 0.5 M; (B) [LiCl] $\simeq$ 0.75 M; (C) [$CaCl_2$] $\simeq$ 1 M; (D) anhydrous Ca^{2+}–DMPS complex. The Ca^{2+} salt of DMPS was prepared according to Bligh and Dyer (1959) and thoroughly dried in vacuo. Chemical shifts are expressed in ppm relative to 85% H_3PO_4.

The effect of $CaCl_2$ on the thermal behavior of bovine brain PS is shown in Figure 4A,B. Ca^{2+} concentrations <0.01 M have no detectable effect on bovine brain PS. At [Ca^{2+}] >0.01 M, a second, broad endothermic transition appears at ~120 °C in addition to the transition at ~14 °C. With increasing Ca^{2+} concentration, the temperature of the low-temperature transition increases slightly, and the enthalpy of the high-temperature transition appears to grow at the expense of that of the low-temperature transition. The T_c of the high-temperature transition varies between 117 and 124 °C. At [$CaCl_2$] = 0.5 M, this transition broadens significantly. In the presence of Ca^{2+}, bovine brain PS also exhibits a low-enthalpy transition at ~50 °C (data not shown).

The thermotropic behavior of POPS is similar to that of bovine brain PS, with respect to both its thermotropic behavior and its interaction with excess Li^+ and Ca^{2+} ions. As shown in Figure 2B, the sharp gel to liquid-crystal transition temperature of the monosodium salt of POPS in sodium phosphate buffer, pH 7.0, occurs at 13.9 ± 0.2 °C (ΔH = 6.8 kcal/mol). Similar behavior is observed with POPS dispersed in 5 mM Tris buffer, pH 7.0. Increasing the Na^+ concentration to 0.5 M has little effect on the thermal behavior of POPS; the transition temperature increases by ~1 °C, and the enthalpy remains essentially constant. High-temperature transitions induced by the addition of excess Li^+ and Ca^{2+} to POPS (data not shown) are similar to those described above for bovine brain PS (see Figures 3 and 4).

The sodium salt of DOPS dispersed in 5 mM phosphate buffer, pH 7, containing 5 mM EDTA, gives an endothermic transition at −11 °C (ΔH = 8.5 ± 0.5 kcal/mol) that is superimposed on the ice-melting peak. Our data (not shown) on DOPS dispersions are in good agreement with those reported by Browning and Seelig (1980). No endothermic transition is observed upon heating unless the DOPS dispersion is frozen during the preceding cooling run. The effect of excess Li^+ on the thermal behavior of DOPS is different from the other PS having saturated or a single cis-unsaturated fatty acyl chain. The transition is broadened, and its temperature increases by a few degrees centigrade, but even at the highest Li^+ concentration (~1 M), no second transition at high tempeature indicative of a Li^+-DOPS complex is observed (data not shown). In contrast to Li^+, DOPS in the presence of excess $CaCl_2$ gives rise to a high-temperature transition at temperatures between 119 and 124 °C. As with other Ca^{2+}–PS complexes, the transition endotherm is followed by an exothermic event [see Hauser and Shipley (1984)]. Sometimes a residual broad endothermic transition is observed at 20–35 °C (range 10–50 °C) (data not shown).

^{31}P NMR. Figure 5 shows proton-decoupled ^{31}P NMR powder spectra recorded at room temperature of aqueous precipitates of different salts of DMPS formed in the presence of excess cations. The ^{31}P powder spectrum of the aqueous

Table II: Spectral Breadth (Expressed as $|\Delta\sigma|$ in ppm) of Metal Ion–PS Complexes[a]

metal ion–PS complex	$\|\Delta\sigma\|$ (ppm)	exptl[b] conditions
Na^+–DMPS	80	ap
Na^+–DMPS	195	anhydrous
Li^+–DMPS	190	ap
Ca^{2+}–DMPS	177 80	ap
Ca^{2+}–DMPS	185	anhydrous
NH_4^+–POPS	55–60	ap
Li^+–POPS	60	ap
Ca^{2+}–POPS	180	ap
Na^+–DOPS	57	ap
Li^+–DOPS	61	ap
Ca^{2+}–DOPS	185 60	ap

[a] The spectral breadth, $|\Delta\sigma|$, is the distance in ppm between the left-hand and the right-hand edge of the spectrum. In axially asymmetric powder spectra, the position of the two edges represents the σ_{11} and σ_{33} component, respectively, of the ^{31}P chemical shielding tensor. In axially symmetric powder spectra, the left-hand edge and the right-hand edge represent the $\sigma_\parallel$ and the $\sigma_\perp$ component of the chemical shielding tensor, respectively. [b] ap, aqueous precipitate. Aqueous precipitates of the metal ion–PS complexes were prepared as described under Methods. The term anhydrous indicates that the aqueous precipitate was thoroughly dried in vacuo; it does not imply that the PS has completely lost its water of hydration.

precipitate of the Na^+ salt of DMPS is characteristic of an axially symmetric ^{31}P chemical shielding tensor, indicating that the phosphate group is still mobile (Figure 5A). In contrast, the aqueous precipitate of Li^+–DMPS gives rise to an axially asymmetric ^{31}P powder spectrum of spectral width $\Delta\sigma \simeq 190$ ppm (Table II) indicative of a rigid headgroup (Figure 5B). The ^{31}P powder spectrum of the Ca^{2+}–DMPS precipitate is complex (Figure 5C). The spectrum can be simulated as the sum of two powder spectra, one characteristic of an axially asymmetric ^{31}P chemical shielding tensor of spectral width of $\sim$177 ppm and one characteristic of an axially symmetric ^{31}P chemical shielding tensor. The width of the latter spectrum is $\sim$80 ppm and very similar to that of the Na^+ salt of DMPS (cf. Figure 5A,C and see Table II). As expected, after the Ca^{2+}–DMPS complex was dried under vacuum, a pure axially asymmetric ^{31}P powder spectrum ($\Delta\sigma \simeq 185$ ppm) results (Figure 5D and Table II).

Aqueous precipitates were also formed from POPS and DOPS in the presence of excess metal ions, and proton-decoupled ^{31}P powder spectra of these PS–metal ion complexes were recorded. Their spectral shapes are similar to those depicted in Figure 5 for DMPS. They are characteristic of either axially symmetric or asymmetric ^{31}P chemical shielding tensor but differ in the spectral width, $\Delta\sigma$, a measure of the anisotropy of motion. Both the NH_4^+ and Li^+ salts of POPS give axially symmetric ^{31}P powder spectra of spectral width 55–60 ppm (Table II). The value of $\Delta\sigma$ of 55–60 ppm for the chemical shielding anisotropy of all the monovalent cation salts of POPS is characteristic of the liquid-crystalline bilayer state. Similar values are also obtained for the monovalent cation salts of bovine brain PS and DOPS (Table II). These values are 20–25 ppm smaller than the chemical shielding anisotropy of Na^+–DMPS (see Figure 5A) which is in the bilayer gel state at room temperature. The decreased motional freedom of the PS polar headgroup below the transition temperature apparently results in a larger chemical shift anisotropy. Our $\Delta\sigma$ values in the absence of metal ions are in good agreement with published data [see Browning and Seelig (1980)]. The aqueous precipitate of Ca^{2+}–POPS gives a pure axially asymmetric ^{31}P powder spectrum of spectral width $\sim$180 ppm (Table II); i.e., there is no significant contribution from an axially symmetric

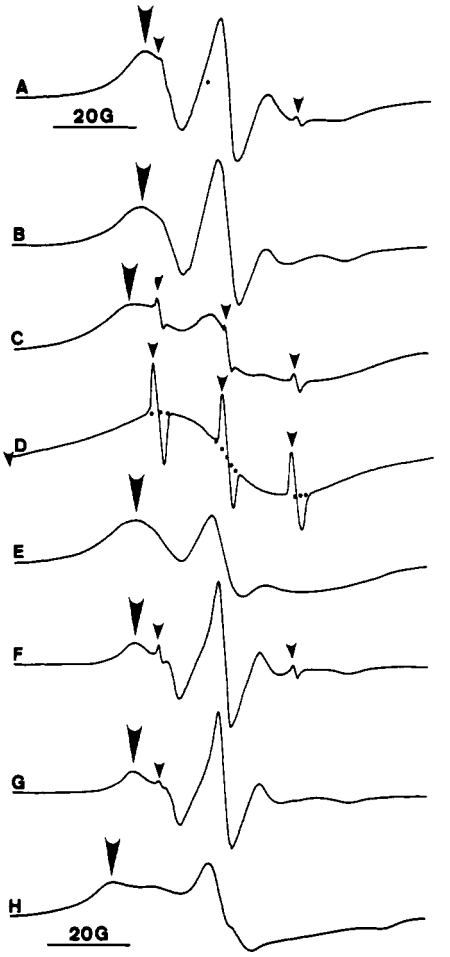

FIGURE 6: First-derivative ESR spectra of unsonicated DMPS or bovine brain PS (Na^+ salt) dispersions in 5 mM Tris buffer, pH 7, labeled with either 8-doxyl-PC or 5-doxylstearic acid. The magnetic field sweep was 100 G, and all spectra were recorded at room temperature (25 °C). Dispersions A–E were DMPS labeled with 8-doxyl-PC; dispersions F–H were bovine brain PS labeled with 5-doxylstearic acid. Where indicated, a large excess of salt was added as described under Materials and Methods. (A) [DMPS–Na^+] $\simeq$ 0.055 M, DMPS/label = 25:1 (mol. ratio); (B) [DMPS–Na^+] $\simeq$ 0.014 M, DMPS/label = 100:1, [LiCl] $\simeq$ 0.5 M; (C) [DMPS–Na^+] $\simeq$ 0.28 M, DMPS/label = 25:1, [LiCl] $\simeq$ 0.75 M; (D) dispersion of pure 8-doxyl-PC (2.7×10^{-4} M) in 5 mM Tris buffer, pH 7; (E) [DMPS–Na^+] $\simeq$ 0.028 M, DMPS/ label = 25:1, [$CaCl_2$] $\simeq$ 1 M; (F–H) [Na^+–bovine brain PS] $\simeq$ 0.025 M, bovine brain PS/label = 50:1, [NaCl] $\simeq$ 0.5 M (F), [LiCl] $\simeq$ 0.75 M (G), and [$CaCl_2$] $\simeq$ 1 M (H).

powder spectrum. This indicates that the conversion to the Ca^{2+} complex with a rigid headgroup is complete. The aqueous precipitates of bovine brain PS obtained with excess Na^+, Li^+, or Ca^{2+} closely resemble the corresponding POPS complexes. Further, similar to POPS, both the Na^+ and Li^+ salts of DOPS give axially symmetric ^{31}P powder spectra with spectral widths of 57 and 61 ppm, respectively (Table II). As discussed for the Ca^{2+}–DMPS complex (see Figure 5C), the Ca^{2+}–DOPS complex gives a mixed powder pattern consisting of two components, an axially asymmetric ^{31}P powder spectrum of spectral width 185 ppm and, superimposed on this, an axially symmetric powder spectrum of spectral width $\sim$60 ppm (Table II).

Electron Spin Resonance. The ESR spectrum of 8-doxyl-PC incorporated in bilayers of the sodium salt of DMPS is shown in Figure 6A. It is characteristic of rapid but anisotropic motion of the spin-label. The value of the maximum hyperfine splitting ($2A_\parallel$) which is a measure of the anisotropy of motion is 48 G. Sometimes a sharp, isotropic three-line

spectrum is superimposed on the anisotropic spectrum (see Figure 6A, C, D, F, and G, small arrows). This sharp, three-line spectrum is probably due to freely tumbling, water-soluble 8-doxyl-PC (or a derivative thereof) that has partitioned into the aqueous phase.

Increasing NaCl concentrations up to 0.5 M have little effect on the ESR spectrum shown in Figure 6A except that the maximum hyperfine splitting $2A_{\parallel}$ increases slightly. Minor effects are also observed with DMPS bilayers labeled with 8-doxyl-PC when LiCl is added up to 0.5 M (Figure 6B). However, when the LiCl concentration is further increased, a spin-exchange broadened spectrum results (Figure 6C). For comparison, the ESR spectrum of a pure 8-doxyl-PC dispersion is shown in Figure 6D. In this case, spin-label molecules are in contact with each other, and consequently, a spin-exchange spectrum is observed; superimposed on it is the sharp three-line spectrum (small arrows) arising from free spin-label as discussed above. Comparing the spectra in Figure 6C,D, it is clear that superimposed on the spin-exchange spectrum in Figure 6C are small contributions from both isotropic (small arrows) and anisotropic spectra (large arrows). In the absence of Li^+ or at [LiCl] $\leq$ 0.5 M, most of the 8-doxyl-PC label is apparently randomly distributed within the DMPS bilayer. At [Li^+] > 0.5 M, the spin-exchange spectrum that is observed is indicative of cluster formation of the spin-label within the crystalline Li^+–DMPS bilayer, a phenomenon which has been referred to as clustering or two-dimensional lateral-phase separation (Hauser & Shipley, 1981). The anisotropic component indicates that probably not all of the 8-doxyl-PC molecules are squeezed out from the Li^+–DMPS bilayer. A spin-exchange broadened ESR spectrum is also observed for DMPS spin-labeled with 8-doxyl-PC in the presence of excess Ca^{2+} (Figure 6E). Again, superimposed on the spin-exchange spectrum in Figure 6E is an anisotropic component. The contribution of this anisotropic component is greater than in the Li^+–DMPS complex (cf. Figure 6C,E). DMPS bilayers labeled with 5-doxylstearic acid behave similarly to DMPS bilayers labeled with 8-doxyl-PC. In the presence of NaCl, ESR spectra resembling that of Figure 6A are obtained, while in the presence of excess Li^+ and Ca^{2+} ions spin-exchange broadened spectra are observed similar to those depicted in Figure 6C,E (data not shown).

The ESR spectra of 5-doxylstearic acid incorporated in bilayers of bovine brain PS in the presence of excess Na^+, Li^+, and Ca^{2+} ions are shown in spectra F, G, and H, respectively, of Figure 6. Similar ESR spectra are observed in the presence of Na^+ and Li^+ (Figure 6F,G); they are characteristic of rapid, anisotropic motion of the spin probe. In both cases, the maximum hyperfine splitting $2A_{\parallel}$ = 52 G. In contrast to the interaction between DMPS and Li^+, this cation apparently does not induce lateral-phase separation in bovine brain PS bilayers: there is no spin-exchange broadening (Figure 6G). In contrast, the Ca^{2+} complex of bovine brain PS gives a spin-exchange broadened spectrum (Figure 6H). As with the Ca^{2+}–DMPS complex, an anisotropic immobilized spectrum is superimposed on the spin-exchange spectrum as indicated by the residual maxima and minima (Figure 6H, large arrows). The value of the maximum hyperfine splitting constant derived from Figure 6H is $2A_{\parallel}$ = 65 G which is close to the value of the hyperfine splitting tensor component A_{zz}. This $2A_{\parallel}$ value indicates that some of the 5-doxylstearic acid is incorporated and randomly distributed in the Ca^{2+}–bovine brain PS bilayer which is presumably crystalline (see Discussion). That the clustering or lateral-phase separation induced by Ca^{2+} is primarily due to the interaction between PS and Ca^{2+} and not between the spin-labeled fatty acid and Ca^{2+} can be readily demonstrated by labeling the PS bilayer with the methyl ester of 5-doxystearic acid. This spin-label has no affinity for Ca^{2+}. DMPS and bovine brain PS bilayers labeled with this spin-label give ESR spectra in the absence and presence of metal ions that closely resemble those obtained with PS bilayers with free fatty acid spin-label.

The metal ion complexes formed between POPS and excess Na^+, Li^+, and Ca^{2+} ions exhibit a similar behavior to that described for bovine brain PS. DOPS labeled with 5-doxylstearic acid gives similar ESR spectra in the presence of excess Na^+ and Li^+ ions. The spectra resemble those of bovine brain PS shown in Figure 6F,G except that the values for the maximum hyperfine splitting, $2A_{\parallel}$ = 50 G, are slightly smaller. In the presence of excess Ca^{2+}, a spin-exchange broadened spectrum is obtained which is practically identical with that shown in Figure 6H.

Discussion

Monolayer Studies. The sodium salts of phosphatidylserines containing 16-carbon saturated chains (DPPS with ester-linked chains and DHPS with ether-linked chains) form condensed monolayers when spread at the air–water interface, while the shorter 14-carbon chain PS (DMPS) undergoes a surface transition from a liquid-expanded to a liquid-condensed monolayer (see Figure 1A). This transition is much broader when DMPS is spread on Tris buffer rather than phosphate buffer. As pointed out previously (Hauser & Shipley, 1983), the Tris counterion probably interacts with negatively charged PS surfaces, thereby affecting the two-dimensional phase transition. The limiting areas per molecule of the saturated PS are all ~40 Å^2. This value is identical with that of saturated-chain phosphatidylethanolamines (PE) but significantly smaller than that of the corresponding phosphatidylcholines (PC) with a bulkier choline-containing polar group (limiting area = 45 Å^2) [see Phillips and Chapman (1968)]. In contrast, Na^+–PS containing cis-unsaturated chains (POPS, DOPS, and bovine brain PS) form only liquid-expanded monolayers over the pressure range studied (see Figure 1A). The PS containing trans-unsaturated chains (DEPS) also exhibits only liquid-expanded monolayers but with a smaller area per molecule and smaller limited area than its cis-unsaturated chain counterpart (cf. DEPS and DOPS in Figure 1A), suggesting that, as expected, the trans-unsaturated chains pack more efficiently than cis-unsaturated chains.

The presence of 100 mM Li^+ in the subphase has little effect on most PS monolayers, the exceptions being DMPS and DEPS. The effect of 100 mM Li^+ on DMPS is to sharpen the two-dimensional, liquid-expanded $\leftrightarrow$ liquid-condensed phase transition, the transition onset being at 8.8 mN/m. This is consistent with the idea that Li^+ in some way stabilizes the condensed monolayer of DMPS via interactions with charged groups at the monolayer surface. It should be said, however, that this interaction (except in the region of the transition; see Figure 1B, curves 2 and 2a) does not lead to significant changes in the molecular area occupied by DMPS in either the condensed or the expanded monolayers (for example, see Table I). Since the other saturated-chain PS (DPPS and DHPS) only form condensed monolayers over the whole pressure range studied (at least at room temperature), it is not surprising that major changes do not occur in their surface behavior in the presence of Li^+. Perhaps Li^+ interacts with DHPS and DPPS in a similar fashion to DMPS (see above), but the monolayer experiments are not revealing.

With the exception of DEPS, the unsaturated-chain PS (POPS, DOPS, and bovine brain PS) exhibit only liquid-ex-

panded monolayers at the temperature studied. While the monolayer data (Table I) sugest no interaction of these PS with Li^+, it should be borne in mind that for Li^+–DMPS, where there is good evidence of a molecular interaction from the effect on the two-dimensional phase transition, again the area of DMPS in the liquid-expanded monolayers is insensitive to the presence of Li^+. For DEPS in the presence of Li^+, a significant monolayer condensation is observed over the whole pressure range, and there is clear evidence of a transition at 25 mN/m. This would suggest that for DEPS, Li^+ triggers a two-dimensional transition, presumably via binding to DEPS polar groups at the interface.

A possible explanation for the behavior of different PS monolayers lies in a selectivity of Li^+ binding depending on the molecular area of the PS. It can be seen that Li^+ apparently interacts better with PS molecules occupying intermediate molecular areas at the interface (DMPS and DEPS) rather than the tightly condensed DPPS and DHPS or more fully expanded POPS, DOPS, and bovine brain PS.

The addition of 10 mM Ca^{2+} to the subphase produced a significant condensation of all PS isotherms (see Figure 1C and Table I), suggesting a strong ionic Ca^{2+}–PS polar group interaction leading to "tighter" molecular packing. It is noticeable (see Table I) that POPS, bovine brain PS, and DEPS exhibit greater condensations in the presence of Ca^{2+} than both the more expanded (DOPS) and less expanded (DMPS, DPPS, and DHPS) PS. Again, this would suggest some selectivity in the interaction of Ca^{2+} with different PS depending on their interfacial area characteristics (see discussion below), with optimal interaction with those exhibiting intermediate areas.

Scanning Calorimetry. Following our detailed studies with saturated-chain PS, we focus here on the thermotropic behavior of unsaturated-chain PS in the absence and presence of the metal ions Na^+, Li^+, and Ca^{2+}. For PS containing a single, cis-monounsaturated chain, POPS, and bovine brain PS, similar behavior is observed. Both exhibit gel → liquid-crystalline bilayer transitions at 13–14 °C which are insensitive to $[Na^+]$ up to 0.5 M. In contrast, Li^+ interacts strongly with both POPS and bovine brain PS as evidenced by the upward shift in transition temperature to >50 °C, and Ca^{2+} produces an even greater shift to ~120 °C. Thus, in bilayer systems, at least, the DSC data suggest that Li^+ and Ca^{2+} interact similarly with disaturated- and monounsaturated-chain PS to produce high-melting bilayers. For DOPS, with two cis-monounsaturated chains, the DSC data indicate that only Ca^{2+} is capable of forming a high-melting, crystalline bilayer. Interestingly, Li^+ has little or no effect on DOPS bilayers.

Thus, it would appear that Ca^{2+} forms high-melting complexes with PS bilayers via a mechanism that shows only limited dependence on the molecular area and packing density of the PS. In contrast, Li^+ shows more pronounced selectivity; Li^+ interacts strongly with disaturated PS and PS with a single cis-monounsaturated chain, but no interaction is observed with the diunsaturated DOPS.

NMR and ESR Spectroscopy. The ^{31}P NMR data provide further evidence for the interaction of metal ions at the polar group of PS. Thus, while Na^+–DMPS shows an axially symmetric ^{31}P spectrum indicative of a mobile phosphate group, addition of Li^+ and Ca^{2+} produces more complex, axially asymmetric powder spectra of much increased spectral width indicative of rigid (presumably crystalline) Ca^{2+}– or Li^+–polar group complexes. This is in agreement with previous ^{31}P NMR studies of Ca^{2+} binding to PS derived from egg phosphatidylcholine (Hope & Cullis, 1980). In the presence of Ca^{2+}, a residual symmetric component is present in the ^{31}P NMR spectra of Ca^{2+}–DMPS, suggesting that at the $[Ca^{2+}]$ used, incomplete conversion to the rigid Ca^{2+}–DMPS phase has occurred. This is indicative of Ca^{2+}-induced phase separation of DMPS bilayers. For POPS and DOPS, identical axially symmetric ^{31}P NMR powder spectra are observed in the presence of NH_4^+ or Li^+, both with a spectral width of 55–60 ppm. Thus, Li^+ does not restrict motional averaging about the bilayer normal. In contrast, Ca^{2+} binding to both POPS and DOPS results in axially asymmetric spectra ($\Delta\sigma$ ~180 ppm) characteristic of a rigid, immobilized phosphate group. In contrast to both saturated (DMPS) and diunsaturated PS (DOPS), the conversion to the rigid, crystalline complex via Ca^{2+} binding appears to be complete only with the monounsaturated PS species (POPS and bovine brain PS) but not with the saturated and diunsaturated PS (see Figure 5).

Samples that give rise to axially asymmetric ^{31}P powder spectra (Figure 5 and Table II) consistently give spin-exchange broadened ESR spectra (Figure 6). This correlation holds for all samples examined in this study. The spin-exchange broadened ESR spectra observed for metal–PS complexes indicate that the metal ion induces a two-dimensional phase separation with most of the spin-label being squeezed out from the metal ion–PS complex. Before the addition of metal ion, the ESR spectra are consistent with the spin-label being uniformly distributed within the host PS bilayers; after the addition of metal ion and the formation of a metal ion–PS complex, most of the spin-label separates out from the host PS bilayer to form patches of spin-label molecules. We note that the detection of spin-exchange broadening depends on the spin-label concentration in the PS bilayer; it is more readily observable the larger the spin-label:PS molar ratio. Spin-exchange broadening is readily detected for DMPS–8-doxyl-PC bilayers at $[Li^+] \geq 0.75$ M and for all PS bilayers labeled with either 8-doxyl-PC or 8-doxylstearate in the presence of excess Ca^{2+} if the PS:spin-label molar ratio is 50.

X-ray diffraction (Hauser & Shipley, 1984) and infrared spectroscopy (Casal et al., 1987a,b) show that PS bilayers differing in the degree of hydrocarbon-chain saturation all crystallize in the presence of excess Ca^{2+}. Thus, the observation of axially asymmetric ^{31}P powder spectra together with the observation of spin-exchange broadening in the ESR spectra from spin-labeled bilayers provides strong evidence that the bilayer is in the crystalline state.

Summary

A consistent pattern of behavior is emerging from the interaction of metal ions (particularly NH_4^+, Na^+, Li^+, and Ca^{2+}) with PS of different chain composition. First, Na^+ and NH_4^+ display only weak interactions with PS monolayers and bilayers; their interactions appear restricted to shielding effects at the PS surface, and no major changes in molecular conformation, chain packing, headgroup dynamics, etc. are apparent. Furthermore, no differential effects have been observed with PS of differing chain composition (disaturated, saturated–unsaturated, diunsaturated).

Second, in contrast, Li^+ interacts strongly with the saturated-chain PS, forming high-melting crystalline Li^+–PS bilayers. An interaction is observed with POPS and bovine brain PS (and DEPS, at least at monolayer surfaces), but Li^+ does not interact with the diunsaturated DOPS. Here it seems reasonable to suggest that there is a gradation in the interaction with Li^+, DMPS > POPS ≃ bovine brain PS > DOPS and that interactions with Li^+ depend to some extent on the molecular area occupied by the PS molecule at the interface, the

separation of adjacent PS molecules, and the surface charge density.

Finally, the divalent cation Ca^{2+} interacts with all PS monolayers and bilayers; the interaction is relatively insensitive to chain composition, although it should be said that Tilcock et al. (1984) provide some evidence for a weaker interaction of Ca^{2+} with the more unsaturated dilinoleoyl-PS. Perhaps in this case the strong, bivalent interactions can more or less override other factors such as molecular area, molecular separation, and surface charge density.

ACKNOWLEDGMENTS

We thank Dr. F. Paltauf for supplying some of the synthetic PS used in this study. We thank Irene Miller for help in preparing the manuscript.

Registry No. DLPS, 76260-76-9; DMPS, 64023-32-1; DPPS, 40290-42-4; DHPS, 118574-54-2; DSPS, 51446-62-9; POPS, 40290-44-6; DOPS, 70614-14-1; DEPS, 63976-14-7; Na^+-DMPS, 105405-50-3; Li^+-DMPS, 118495-76-4; Ca^{2+}-DMPS, 118495-77-5; NH_4^+-POPS, 111001-23-1; Li^+-POPS, 118574-55-3; Ca^{2+}-POPS, 118574-56-4; Na^+-DOPS, 90693-88-2; Li^+-DOPS, 118574-57-5; Ca^{2+}-DOPS, 118574-58-6; Na, 7440-23-5; NH_4^+, 14798-03-9; Li, 7439-93-2; Ca, 7440-70-2.

REFERENCES

Abramson, M. B., Katzman, R., & Gregor, H. P. (1964) *J. Biol. Chem. 239*, 70–76.

Atkinson, D., Hauser, H., Shipley, G. G., & Stubbs, J. M. (1974) *Biochim. Biophys. Acta 339*, 10–29.

Bligh, E. G., & Dyer, W. J. (1959) *Can. J. Biochem. Physiol. 37*, 911–917.

Browning, J. L., & Seelig, J. (1980) *Biochemistry 19*, 1262–1270.

Casal, H. L., Mantsch, H. H., & Hauser, H. (1987a) *Biochemistry 26*, 4408–4416.

Casal, H. L., Martin, A., Mantsch, H. H., Paltauf, F., & Hauser, H. (1987b) *Biochemistry 26*, 7395–7401.

Cevc, G., Watts, A., & Marsh, D. (1981) *Biochemistry 20*, 4955–4965.

Comfurius, P., & Zwaal, R. F. A. (1977) *Biochim. Biophys. Acta 488*, 36–42.

Eisenberg, M., Gresalfi, T., Riccio, T., & McLaughlin, S. (1979) *Biochemistry 18*, 5213–5223.

Feigenson, G. W. (1986) *Biochemistry 25*, 5819–5825.

Hauser, H., & Phillips, M. C. (1973) *J. Biol. Chem. 248*, 8585–8591.

Hauser, H., & Shipley, G. G. (1981) *J. Biol. Chem. 256*, 11377–11380.

Hauser, H., & Shipley, G. G. (1983) *Biochemistry 22*, 2171–2178.

Hauser, H., & Shipley, G. G. (1984) *Biochemistry 23*, 34–41.

Hauser, H., & Shipley, G. G. (1985) *Biochim. Biophys. Acta 813*, 343–346.

Hauser, H., Finer, E. G., & Darke, A. (1977) *Biochem. Biophys. Res. Commun. 76*, 267–274.

Hauser, H., Paltauf, F., & Shipley, G. G. (1982a) *Biochemistry 21*, 1061–1067.

Hauser, H., Gains, N., Semenza, G., & Spiess, M. (1982b) *Biochemistry 21*, 5621–5628.

Hermetter, A., Paltauf, F., & Hauser, H. (1982) *Chem. Phys. Lipids 30*, 35–45.

Hope, M. J., & Cullis, P. R. (1980) *Biochem. Biophys. Res. Commun. 92*, 846–852.

Jacobson, K., & Papahadjopoulos, D. (1975) *Biochemistry 14*, 152–161.

Loosley-Millman, M. E., Rand, R. P., & Parsegian, V. A. (1982) *Biophys. J. 40*, 221–232.

Luna, E. J., & McConnell, H. M. (1977) *Biochim. Biophys. Acta 470*, 303–316.

MacDonald, R. C., Simon, S. A., & Baer, E. (1976) *Biochemistry 15*, 885–891.

McLaughlin, A. C. (1982) *Biochemistry 21*, 4879–4885.

McLaughlin, S., Mulrine, N., Gresalfi, T., Vaio, G., & McLaughlin, A. (1981) *J. Gen. Physiol. 77*, 445–473.

Newton, C., Pangborn, W., Nir, S., & Papahadjopoulos, D. (1978) *Biochim. Biophys. Acta 506*, 281–287.

Ohki, S., & Kurland, R. (1981) *Biochim. Biophys. Acta 645*, 170–176.

Ohki, S., Duzgunes, N., & Leonards, K. (1982) *Biochemistry 21*, 2127–2133.

Paltauf, F., Hauser, H., & Phillips, M. C. (1971) *Biochim. Biophys. Acta 249*, 539–547.

Papahadjopoulos, D., & Miller, N. (1967) *Biochim. Biophys. Acta 135*, 624–638.

Papahadjopoulos, D., Vail, W. J., Newton, C., Nir, S., Jacobson, K., Poste, G., & Lazo, R. (1977) *Biochim. Biophys. Acta 465*, 579–598.

Papahadjopoulos, D., Portis, A., & Pangborn, W. (1978) *Ann. N.Y. Acad. Sci. 308*, 50–63.

Phillips, M. C., & Chapman, D. (1968) *Biochim. Biophys. Acta 163*, 301–313.

Pines, A., Gibby, M. G., & Waugh, J. S. (1973) *J. Chem. Phys. 59*, 569–590.

Puskin, J. S. (1977) *J. Membr. Biol. 35*, 39–55.

Tilcock, C. P. S., Bally, M. B., Farren, S. B., Cullis, P. R., & Gruner, S. M. (1984) *Biochemistry 23*, 2696–2703.

van Dijck, P. W. M., de Kruijff, B., Verkleij, A. J., van Deenen, L. L. M., & de Gier, J. (1978) *Biochim. Biophys. Acta 512*, 84–96.